

Article

Flood Risk Mapping Using LiDAR for Annapolis Royal, Nova Scotia, Canada

Tim L. Webster

Applied Geomatics Research Group, Nova Scotia Community College, Middleton, Nova Scotia B0S 1M0, NS, Canada; E-Mail: timothy.webster@nsc.ca; Tel.: +1-902-825-2775; Fax: +1-902-825-5479

Received: 10 July 2010; in revised form: 19 August 2010 / Accepted: 20 August 2010 /

Published: 1 September 2010

Abstract: A significant portion of the Canadian Maritime coastline has been surveyed with airborne Light Detection and Ranging (LiDAR). The purpose of these surveys has been to map the risk of flooding from storm surges and projected long-term sea-level rise from climate change and to include projects in all three Maritime Provinces: Prince Edward Island, New Brunswick, and Nova Scotia. LiDAR provides the required details in order to map the flood inundation from 1 to 2 m storm surge events, which cause coastal flooding in many locations in this region when they occur at high tide levels. The community of Annapolis Royal, Nova Scotia, adjacent to the Bay of Fundy, has been surveyed with LiDAR and a 1 m DEM (Digital Elevation Model) was constructed for the flood inundation mapping. Validation of the LiDAR using survey grade GPS indicates a vertical accuracy better than 30 cm. A benchmark storm, known as the Groundhog Day storm (February 1–3, 1976), was used to assess the flood maps and to illustrate the effects of different sea-level rise projections based on climate change scenarios if it were to re-occur in 100 years time. Near shore bathymetry has been merged with the LiDAR and local wind observations used to model the impact of significant waves during this benchmark storm. Long-term (*ca.* greater than 30 years) time series of water level observations from across the Bay of Fundy in Saint John, New Brunswick, have been used to estimate return periods of water levels under present and future sea-level rise conditions. Results indicate that under current sea-level rise conditions this storm has a 66 year return period. With a modest relative sea-level (RSL) rise of 80 cm/century this decreases to 44 years and, with a possible upper limit rise of 220 cm/century, this decreases further to 22 years. Due to the uncertainty of climate change scenarios and sea-level rise, flood inundation maps have been constructed at 10 cm increments up to the 9 m contour which represents an upper flood limit estimate in 100 years, based on the highest predicted tide, plus a 2 m storm surge and a RSL of 220 cm/century.

Keywords: LiDAR; flood inundation; flood risk; water levels; DEM

1. Introduction

Generally, Digital Elevation Models (DEMs) derived from aerial photography or other remote sensing systems such as the Shuttle Radar Topography Mission (SRTM) have degraded accuracies in forested areas. In Maritime Canada, previous topographic maps derived from aerial photo surveys were hampered in forested areas where the ground was obscured by trees and accurate measurements of the terrain were difficult (<http://www.gov.ns.ca/snsmr/land/programs/post/manual/default.asp>). Light Detection and Ranging (LiDAR) is a remote sensing technology to derive very accurate elevation measurements of the earth's surface. Flood *et al.* and Wehr *et al.* [1,2] provide a general overview of airborne laser scanning (LiDAR) technology and principles. The benefit of LiDAR is that a narrow laser beam is directed from the aircraft towards the earth's surface and reflected back in order to measure the range or distance from the aircraft to the ground. The beam divergence is typically very small (0.3 mrad), resulting in a laser footprint diameter of 20–30 cm on the ground, depending on flying height. Only a portion of that beam has to make it through the gaps in the forest canopy and hit the ground in order to be reflected back to the aircraft. Thus in the forest, if one can see patches of sky above them, there is a good chance the laser beam will partially make it through a gap and make it to the ground or near ground features such as dense shrubs. The LiDAR sensor records a series of points that represent what the laser pulse was reflected off and contains “hits” from the vegetation, buildings, and bare ground targets, for example. Sensors in the 1990s could record the first or last returning laser pulse and eventually evolved to record first and last pulse and the intensity of the backscattered energy. Sensors today are capable of recording intermediate pulse returns in addition to the first and last return.

In order to derive an accurate DEM, the LiDAR points are classified or filtered into ‘ground’ and ‘non-ground’ target classes. A critical review of ground classification is presented by [3] where they discuss the criteria for selecting the most appropriate filtering algorithm. They also describe where all of the algorithms are suboptimal: rough terrain or discontinuous slope, dense forest areas where the beam cannot penetrate to the ground, and low vegetation being confused with the ground. The classification methods are categorized into the following groups: segmentation or clustering, morphological, directional scanning, contour, Triangular Irregular Network (TIN), and Interpolation [3]. Kraus *et al.* [4,5] utilized a least squares interpolation method to iteratively remove trees and generate a ground surface. Vosselman [6] applied an approach that compares the slope between a LiDAR point and its neighbor to determine if it is ground or not where a threshold is used to evaluate the slope angle. Axelsson [7] described a method where seed low points are selected within a grid of user-defined size greater than the largest non-ground features. These points are used to construct an initial TIN. Then each point is added to the TIN if the parameters are below the threshold settings. The problem is that different thresholds are required for different terrain conditions. Zhang *et al.* [8] converted the LiDAR points to a raster and then use mathematical morphology filter on the grayscale image to extract ground and non-ground points. They progressively increase the size of the filter

window where different threshold parameters are applied to detect ground and non-ground features. They first generate a minimum elevation surface from the LiDAR points. In the next iteration, they increase the window and apply threshold parameters to form a smoother surface which is subtracted from the previous to identify non-ground points. The current industry standard for processing LiDAR is TerraScan from Terrasolid to process and classify the points. This method is based on the TIN construction from a set of low seed points initially and then iteratively evaluates additional points based on a set of parameters including slope and triangle edge length. Raber *et al.* [9] optimized the parameter settings of this software for different land covers and also used traditional parameter settings and then compared the accuracy of the derived Digital Terrain Models (DTMs). They found the differences were small although statistically significant. Hodgson *et al.* [10] compared LiDAR points and interpolated surfaces from TINs with validation points for different land cover types. Their results indicated that errors varied by land cover type and found that the TIN process did not introduce additional error; in fact it reduced the error in some cases.

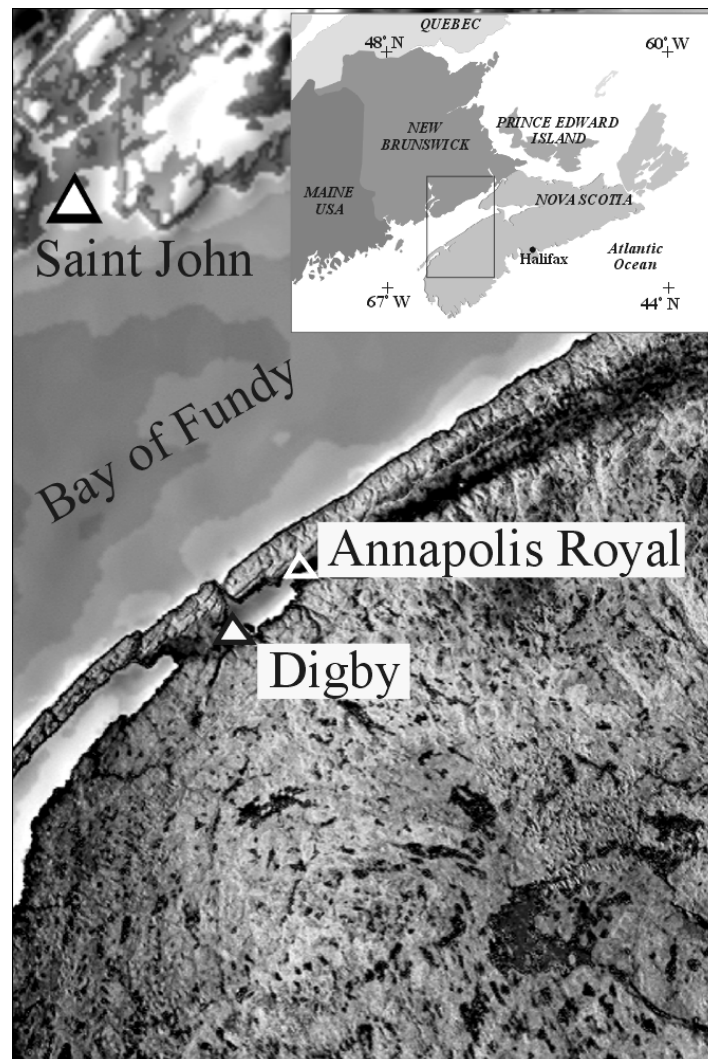
LiDAR has been used in a variety of flood inundation applications involving rivers [11-16]. The research has mainly focused on assessing the impact of LiDAR derived surface model resolution on model results [12,14,16] or on the impact of vegetation and building extraction for urban areas [13,15]. The application of LiDAR to coastal areas has focused on modeling inundation from storms and sea-level rise [17-25]. A good review of LiDAR calibration, validation and processing and a summary of how LiDAR can be used in coastal research to assess geohazards were provided by [17]. They found that the rate and extent of coastal inundation were dependent on LiDAR horizontal grid resolution which also affected assumptions about connectivity of the ocean to low lying inland areas. Many countries that have a significant coastline are using LiDAR to monitor and model surface processes including shoreline mapping and change detection [26-32]. The Atlantic Coast of Canada is considered vulnerable to sea-level rise [33]. The communities of Charlottetown and the north shore of Prince Edward Island (PEI) were mapped for vulnerability to storm surge flooding and long-term sea-level rise [34]. A large storm surge impacted the area in January of 2000 and was used as a benchmark to test the inundation model developed within the ArcGIS system [18,22]. LiDAR was instrumental in facilitating accurate flood risk maps in the PEI study [18,21,34]. The PEI study was followed by a project in southeast New Brunswick that involved the acquisition of LiDAR along 175 km of shoreline for flood risk mapping [20]. The LiDAR surveys were conducted in 2003 and 2004 ensuring that the areas were captured during leaf-off conditions and prior to significant snow cover. A large coastal dune system, La dune de Buctouche, was surveyed in both years and was impacted by a storm in February of 2004. Following similar methods described in [26-32] this multi-temporal LiDAR dataset was used to measure coastal erosion [20].

The third assessment report from the Intergovernmental Panel on Climate Change (IPCC) indicates that there will be an increase in mean global sea-level from 1990 to 2100 between 0.09 m and 0.88 m [35]. Previous flood risk mapping projects from climate change sea-level rise in the region have used the central value of 0.5 m/century to project global sea-level rise into the future [18,20-23]. The latest IPCC Assessment Report 4 (AR4) has projected global mean sea-level to rise between 0.18 and 0.59 m from 1990 to 2095 [36,37]. However, as Forbes *et al.* [38] pointed out, these projections do not account for the large ice sheets melting as not enough literature on the subject was available at the time of the AR4 report. Recent sea-level observations were compared with the IPCC projections from

2001 [39]. The results indicated that sea-level may be responding quicker than the climate models predicted. Observations were based on tide gauge measurements and satellite altimetry. The satellite data show a linear trend (1993–2006) of 33 cm/century. The effects of fresh melt water from ice sheets on the thermohaline circulation (THC) pattern, changes sea-levels regionally and modeling results indicate the North American Atlantic coast could see an increase in sea-level between 0.5 and 1 m as the THC shuts off [40]. Comparison of altimetry data from the Topex-Poseidon satellite between 1993 and 2003 with tide gauge measurements is consistent with a weakening of the THC [40]. Sea-level changes cannot yet be predicted with confidence using models based on physical processes, because the dynamics of ice sheets and glaciers and, to a lesser extent, that of oceanic heat uptake is not sufficiently understood. The correlation between sea-level and temperature is >0.99 for observations from 1880 to 2000 [41]. Climate models predict global mean temperature with confidence and these results were used to estimate sea-levels [41,42]. The future global temperature scenarios based on the PICC AR4 report were used to estimate global sea-level rise between 75 and 190 cm for the period of 1990–2100 [41]. Due to the uncertainty in the global sea-level predictions, [38] used the upper limit of 1.3 m as a precautionary approach to sea-level rise projections in the Halifax region.

Communities around the Bay of Fundy, including Annapolis Royal, are vulnerable to coastal flooding from storm surge events such as the Saxby Gale of 1869 [44,46-49]. The Saxby Gale storm surge could have reached land elevations of between 6.2 and 6.5 m if it were to occur today on a perigean tide, without even considering the relative sea-level rise that has occurred since 1869 [44]. The more recent Groundhog Day storm on February 2, 1976 has been used as the benchmark storm to assess the model results and estimate wave run-up [45,48,50]. The tide gauge at Digby, 50 km southwest of Annapolis Royal, was not operating during the Groundhog Day storm and could not be used to assess the height of the storm surge of this event. However, water levels from the tide gauge at Saint John, New Brunswick, directly across the Bay of Fundy, were used to determine the height of the storm surge during this event and are discussed later in the methods section (Figure 1). The effects of the storm could have been much worse if it had occurred at the highest predicted astronomical tide, which was one meter higher than the tide predicted during the Goundhog Day storm. The tide gauge data from Saint John, NB, were analyzed for this event by [47], who reported a 1.46 m storm surge on top of a mean higher water level of 7.71 m (above chart datum), and stated that the damage would have been worse if the storm had occurred on a perigean spring tide, which recorded water levels of 8.84 m on April 16th, 1976.

Figure 1. Location of the study area, Annapolis Royal, and the nearest long-term tide gauge; Saint John. Digby is directly west of the Annapolis Royal label on the figure.



A previous study [44] indicated that there are several key locations around the town of Annapolis Royal, Nova Scotia, that are susceptible to flooding as a result of storm surges. As a result of that study, flood risk mapping was integrated in a recent Climate Change and Adaptation project, funded by Natural Resources Canada (http://adaptation.nrcan.gc.ca/projdb/178_e.php). In this study, a LiDAR derived DEM of Annapolis Royal, Nova Scotia, was used to construct flood inundation maps based on sea-level rise and climate change (Figure 1). Similar to other flood risk mapping projects in the region [18-23], still water levels were used within the GIS to inundate the land. In these past studies, the return period of the inundation water levels was calculated using 40 years worth of tide gauge records for the region [43]. Bernier *et al.* [43] recently compared the return period of storm surges and total water level from tide gauge records for the region, to the Dalhousie storm surge model driven by 40 years of wind observations and inferred atmospheric pressure fields. In this study, the flood inundation mapping has been coupled with a risk assessment tool, the Water Modeler, to determine return periods of water levels under current conditions and with sea-level rise rates from climate change. The return periods generated by the Water Modeler are compared to those produced by [43]. As a result of uncertainties in future sea-level rise rates, flood inundation maps have been constructed

at 10 cm increments so that as sea-level rise estimates become refined in the future, the appropriate water level inundation map is available. As with previous regional studies [18-23], a benchmark storm from the past has been used to assess the model. In addition to the increased water levels associated with a storm surge (regional scale effect), strong winds associated with a storm blowing on shore can increase wave heights and cause water levels to increase. As waves push toward the shore, the effect of breaking waves produces wave setup, and individual breaking waves produce wave run-up. Wave run-up is more of a local phenomenon that is controlled by the wind speed, wind direction, and the local offshore bathymetry depth and shoreline geometry. Thus, in addition to modeling still water levels, the wave run-up has been estimated for the benchmark storm by utilizing the SWAN model [45] with a seamless DEM which integrated the LiDAR and bathymetric chart data of the basin. The objectives of this study were: (1) utilize a LiDAR derived DEM for flood inundation mapping and assess its accuracy; (2) construct flood risk maps that the community can use to adapt to rising sea-levels; (3) merge the LiDAR DEM with bathymetric data to generate wave run-up predictions based on a historic benchmark storm; and (4) construct return periods of water levels for current and projected sea-level rise conditions and map the water inundation using the LiDAR DEM.

2. Methods

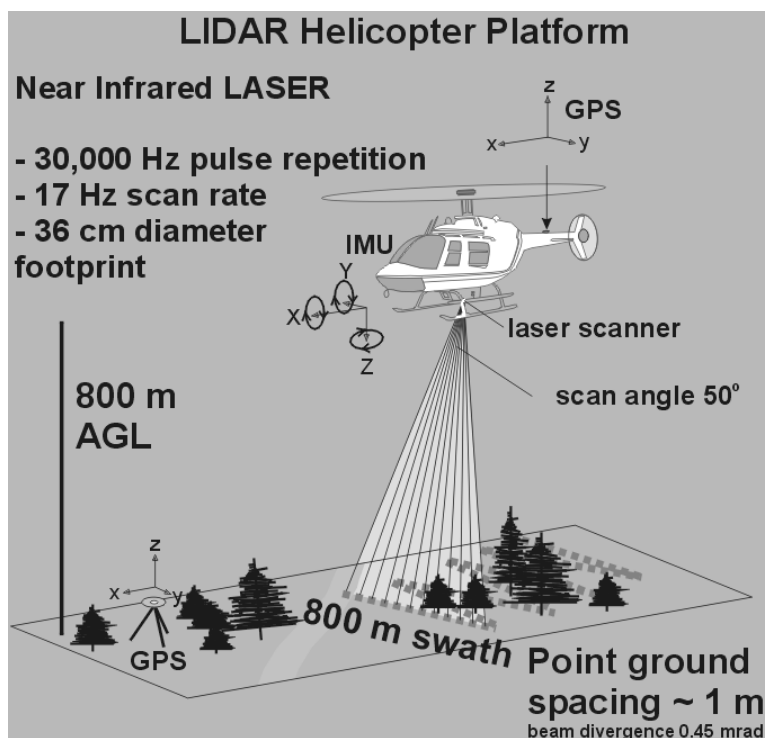
2.1. Airborne LiDAR

LiDAR data were acquired for the study area on April 20–25, 2004 and covered an area of 595 km² as part of the AGRG study of coastal processes along the Nova Scotia shoreline of the Bay of Fundy [19]. The survey was conducted under contract to Terra Remote Sensing Inc. utilizing their Mark II LiDAR system. The area was surveyed at low tide in order to capture the elevation of the exposed inter-tidal zone. The LiDAR system recorded the first and last laser returns with a posting every 1 m on the ground with vertical precision of 15 cm (Figure 2). The Mark II system was mounted on a pod that was fixed to the underside of a Bell 206L helicopter (Figure 2). Since the Mark II could only record intensity of one of the returns (first or last), it was decided to acquire the intensity on alternating returns; thus, every other first and last return would have the intensity recorded. The system utilizes a laser with a wavelength of 1,064 nm and beam divergence of 0.45 mrad, and operated at a 30,000 Hz laser repetition rate, along with the scanning mirror operating at 17 Hz to direct the laser pulses across the swath. The survey was flown at an altitude of 800 m which resulted in a laser footprint diameter of 36 cm (Figure 2). The point spacing was approximately 1 m in the along track and across track direction (Figure 2). The point density increased to near 0.5 m where the flight lines overlapped.

The point cloud was classified utilizing the TerraScan™ software into ‘ground’ and ‘non-ground’ points by the service provider who did not provide the parameters used in the ground classification process. The LiDAR points were processed to have heights relative to the Canadian Geodetic Vertical Datum of 1928 (CGVD28) which is a close approximation of mean sea-level (MSL). The data were delivered in 2 km × 2 km tiles as ASCII files where each point contained the following attributes: UTM easting, UTM northing, ellipsoidal height (relative to GRS80), orthometric height (referenced to CGVD28), GPS time, echo code, flight line number, and intensity. The data were processed into ArcInfo™ GIS point coverages, and different surfaces were constructed. In this study, four surfaces

were constructed using a triangular irregular network algorithm with linear interpolation to a 1 m grid: (1) a “bare-earth” DEM; (2) a digital surface model (DSM) incorporating ‘ground’ and ‘non-ground’ points *i.e.* trees and buildings; (3) a normalized height model which is derived from the subtraction of the DEM from the DSM (height of trees and buildings); (4) an intensity image derived from the ‘ground’ and ‘non-ground’ hits. These surfaces have been used to classify the land cover of the area using an object-orientated classification method [51].

Figure 2. LiDAR configuration for the April 2004 survey.



2.2. LiDAR Validation

The LiDAR points and surfaces were expected to have an absolute vertical error of less than 30 cm, and typically less than 15 cm. Independent survey-grade GPS checkpoints were collected over paved surfaces to validate the LiDAR points and derived surface models. The real-time kinematic (RTK) GPS surveys were conducted using a Leica GPS System 500, where baselines were kept below 15 km in length, allowing the RTK GPS rover to achieve a vertical precision of 3 cm or better. The GPS data were post-processed and orthometric heights were computed and used to compare with the LiDAR points and surfaces following methods described in [52,53]. The LiDAR ground classification was assessed visually and by comparing the DSM and DEM surface models and found to be satisfactory. Extra attention was paid along the coastal zone as these areas are prone to classification errors as a result of the steep slopes and some anthropogenic features (e.g., wharfs).

2.3. Seamless DEM Construction & Wave Modeling

Bathymetric soundings for the Annapolis Basin and river south of Annapolis Royal from the Canadian Hydrographic Service (CHS) Chart 4396 were used to construct a grid that was transformed

from chart datum (typically a value lower than the average lowest tide over a 19 year tidal astronomical cycle) to CGVD28 and merged with the LiDAR DEM and DSM to form “seamless” elevation models. Chart datum is 4.39 m below CGVD28 for Digby. In order to model wave heights, the wind direction and speed must be known as well as local bathymetry. Wave heights were predicted with the SWAN (Simulating WAVes Nearshore) model [45]. The seamless DEM (bathymetry + land) and the predicted tide height (orthometric height of 4.1 m) during the Groundhog Day storm was used as the initial water level. Hourly wind information recorded by Environment Canada at Greenwood, NS (approximately 100 km northeast along the Annapolis Valley) was used to drive the SWAN model [45]. The model was run for 15-minute increments from February 1–3, 1976, and hourly wave height predictions were output at a horizontal grid resolution of 40 m that have been resampled to 10 m and imported into the GIS. The significant wave height that occurs along the shore was added to the storm surge water level in order to determine the area inland affected by wave run-up.

2.4. Observed and Predicted Sea-Levels

Observed hourly water levels were acquired from the Marine Environmental Service (MEDS) website (<http://www.meds-sdmm.dfo-mpo.gc.ca>) for Saint John, NB and Digby, NS (located within Annapolis Basin south of Annapolis Royal) and predicted tide water levels for these sites were acquired (<http://tbone.biol.sc.edu/tide/>). The tide gauge records at Digby only cover 15 months from 1969 to 1970, while the Saint John records span over 30 years from 1966 to 2004. In order to generate return periods for high water levels, 30 years of observations are recommended [23]. The water level record at Digby was not of sufficient length to calculate return periods with any confidence, so the record at Saint John was used in Water Modeler to generate return periods. In order to evaluate the relationship of water levels observed in Saint John with those in the Annapolis Basin (Digby), the tide gauge water level records were examined to find times when both sites were operating simultaneously and the residuals (storm surge events) were calculated for each site by subtracting the predicted water level from the observed water level. The difference in storm surges between the two sites was calculated and statistics generated in order to quantify how similar the sites were. This was used to estimate the uncertainty of the return period of high water events in the Annapolis Basin.

2.5. Sea-Level Rise from Climate Change Estimates

The Saint John tide gauge information indicates that the sea-level has been rising at a rate of 36 cm per century [47]. The International Panel on Climate Change (IPCC) predicts global sea-level to continue to rise [35-37]. In this study, flood inundation maps were calculated up to the 9 m contour level on land as a precautionary approach. In order to calculate return periods on different water levels in the future, a modest rate of 0.5 m per century was used to estimate long-term sea-level rise. As the estimates of sea-level rise from climate change are revised and refined in the future, the return period of any given water level can easily be calculated using the new estimate.

In addition to global sea-level rise, local crustal dynamics also affect relative sea-level. The major influence on crustal motion for this region relates to the last glaciation that ended *ca.* 10,000 years ago [33,54]. The areas where the ice was thickest were depressed the most, and peripheral regions were uplifted, termed the “peripheral bulge”. The ice was thickest over Hudson Bay in central Canada,

where the crust was most depressed; even today this area is still rebounding from the load of the ice and continues to uplift. The Maritimes represent part of the peripheral bulge and southern New Brunswick and Nova Scotia are subsiding [54]. Subsidence rates vary across the region with this area of Nova Scotia sinking at a rate of ~20 cm per century [54]. The subsidence of the crust is important for coastal communities in that it compounds the problem of local sea-level rise and must be considered when projecting future flood risk.

The Bay of Fundy tidal range is expected to increase by 10 cm in the future with an increase in sea-level [55]. When all of these factors are combined, global sea-level rise, crustal subsidence, and tidal amplitude, a potential increase in relative sea-level of 80 cm in the next century is probable. This number will be used to determine the water level of storms, such as the Groundhog Day storm of 1976, should they occur in the future. If one considers the estimates by [40-42], global sea-level could rise by as much as 190 cm over the next century, thus decreasing the return periods of any given water level. With the high level of uncertainty involved in the estimates of global sea-level rise over the next century, flood inundation levels were mapped at every 10 cm up to 9 m. However, instead of determining the return period for several different future sea-level rise estimates which are highly uncertain, I have calculated it for the present relative sea-level rise rate (36 cm/century), and for the estimated rate of 80 cm/century based on the conservative global estimate of 50 cm/century, and for the extreme estimated rate of global sea-level rise of 190 cm/century [41], thereby producing a relative sea-level rise rate of 220 cm/century.

2.6. Flood Inundation Mapping

Water levels were converted from chart datum to CGVD28 (DEM datum), and used to raise the water level of the Annapolis Basin to inundate low-lying areas connected to the basin. In order to ensure that only low-lying areas are flooded that are connected to the basin, care must be taken to determine the extent of culverts and bridges that allow sea water to flow landward. A manmade barrier such as a raised roadbed or railway will be represented on the LiDAR DEM in a similar way as a dyke or levee. The main differences between these features relates to the control and direction of the drainage. Streams and ditches landward of a dyke are often drained by a one-way culvert, or aboiteau, thus not allowing the ocean in at high water levels. However, roads and railways are typically equipped with culverts or bridges to drain the land and allow the ocean to flow landward at high water levels. In order to effectively automate mapping the flood extent in a GIS, the DEM was modified to allow hydraulic pathways for flow through the road and rail beds, in order to connect upstream areas with the ocean following the method of [20]. Once the DEM had the appropriate pathways to allow the flow of water, a water level associated with a tide and storm surge was mapped, based on land elevations and the flood water extent determined. This assumed a flat planar water surface (still water) when projecting a given water level landward. An Arc script has been developed to raise the water level in 10 cm increments, ensuring only areas are flooded that are connected to the basin [22]. The range of water levels that have been used in this study are between -4 m and 9 m above CGVD28. The upper limit of 9 m was selected to accommodate the highest astronomical tide of 4.8 m, plus relative sea-level rise of 2.2 m in the next century (0.2 m crustal subsidence + 0.1 m tidal amplitude + 1.9 m extreme estimate of global sea-level rise [41]), plus a 2 m storm surge and wave-setup combination. The

flood inundation maps were then assigned a probability of occurrence or a return period in years for each water level to assess the risk of flooding using the method outlined in [23].

3. Results

3.1. LiDAR Validation and Surface Construction

The LiDAR ‘ground’ and ‘non-ground’ points were used to construct triangulated irregular networks (TINs) based on the orthometric height that was linearly interpolated to a 1-m resolution digital surface model (DSM) (Figure 3). The ground points were used to construct a second grid using the same method that represented a “bare-earth” digital elevation model (DEM) (Figure 3).

The RTK GPS points were compared to the LiDAR points within a 2 m horizontal distance resulting in a mean difference of 10 cm and a standard deviation of 12 cm, indicating the LiDAR data was within the vertical accuracy expected. The LiDAR DEM was also compared to the GPS points resulting in a mean difference of 4 cm and a standard deviation of 32 cm. The chart bathymetric information was converted to CGVD28 and merged with the LiDAR to construct a seamless DEM for wave modeling with SWAN [54] (Figure 3).

Figure 3. LiDAR surface models. Top: DSM; Middle: DEM; Bottom: seamless DEM comprised of LiDAR for the land and intertidal zone and bathymetric soundings from a chart. Blue shades are below mean sea level and elevation increases from green to red in color.

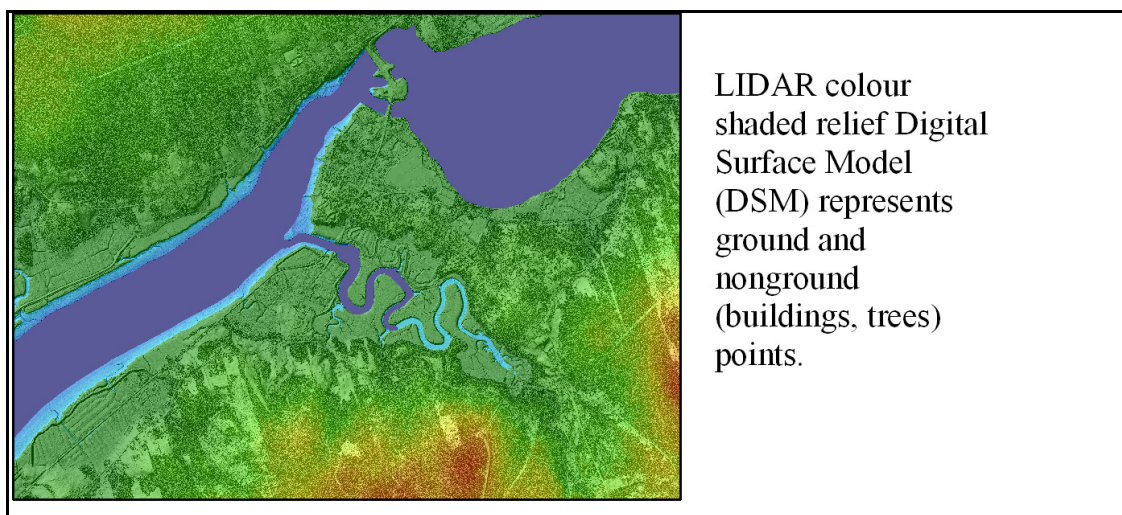
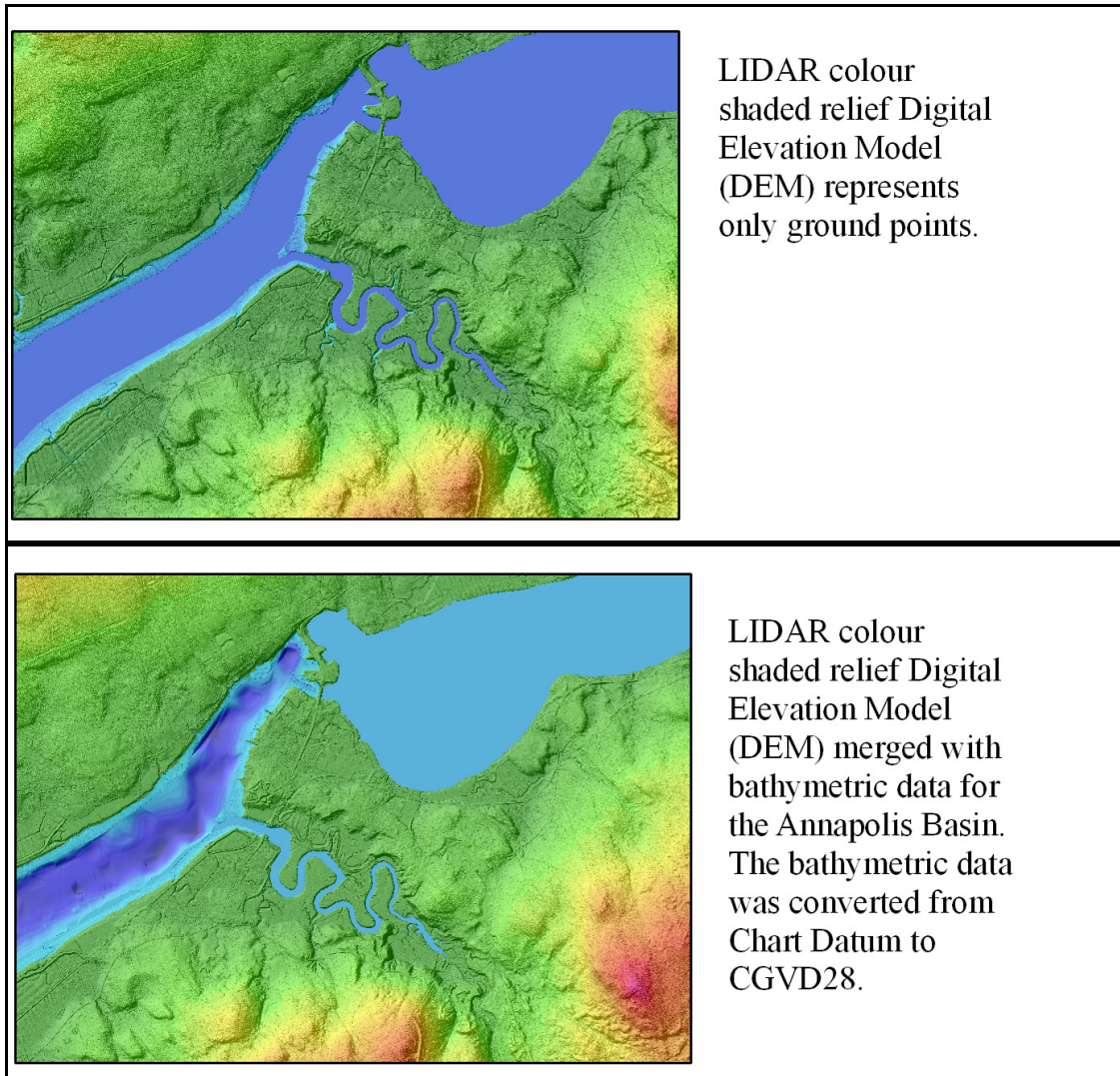


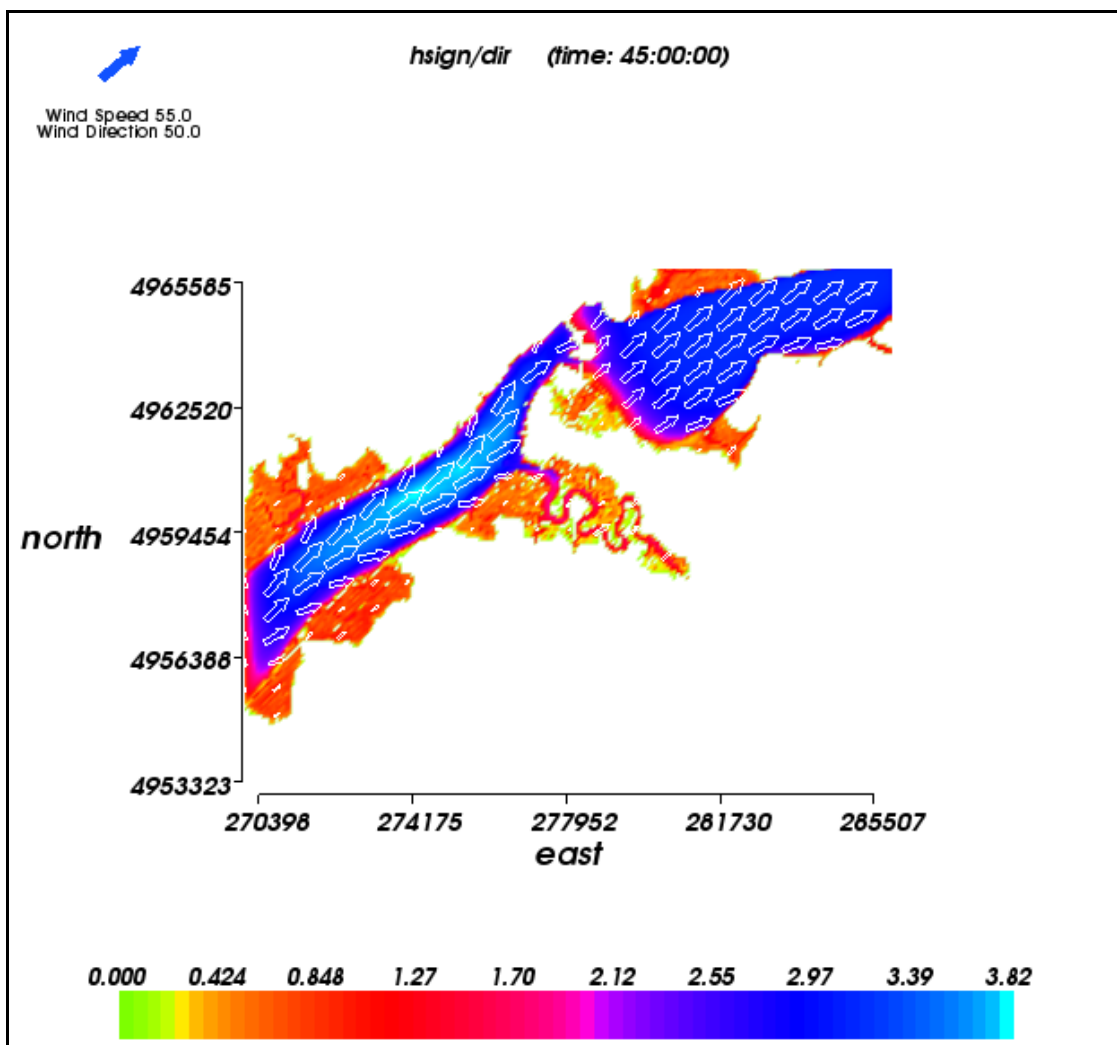
Figure 3. Cont.



3.2. Wave Modeling of the Benchmark Storm

The results of the wave modeling for the Groundhog Day storm for Annapolis Royal show that significant waves were generated in the Annapolis Basin that impacted the shoreline. The water level used for this simulation corresponded to an orthometric height of 4.1 m which represents the predicted tide. Modeled significant wave height along the shore of Annapolis Royal resulted in approximate heights of 2 m, with the largest waves occurring in the channel, calculated to have peak heights greater than 3 m (Figure 4). With the water level set to 4.1 m, much of the low lying area landward of the dykes was flooded and waves generated. This model does not consider connectivity of the ocean to low lying areas separated by dyke structures. Thus the wave heights landward of the dykes were not considered to be accurate because according to the LiDAR-based flood inundation mapping, the dykes on the east and west side of the basin, southwest of Annapolis Royal, were not overtopped by a 4.1 m water level. However, the significant wave heights near Annapolis Royal appear to agree with newspaper reports of waves overtopping the causeway.

Figure 4. Results from the SWAN wave model. The model represents the maximum significant wave heights generated for winds from Greenwood, NS, February 1–3, 1976 and a water level set to 4.1 m, which represents the predicted tide. The colors represent the significant wave height (m) and white arrows represent the direction and size of the waves. The blue arrow in the upper left represents the speed (km/hr) and direction of the wind. Coordinates along the side are UTM Zone 20 NAD83 easting and northing values.



3.3. Observed Water Level Residuals (Storm Surges) between Sites

In order to examine the relationship between water levels in Saint John and those in the Annapolis Basin, the observed water level records at Saint John and Digby for the period of January to March, 1970, have been analyzed. The predicted water level for each site has been determined and combined with the observed water levels and residuals (storm surge) calculated during this period (Figure 5). Generally, the storm surges observed in Saint John are observed in Digby nearly concurrently. This is not surprising, considering the scale of the weather systems (low pressure and associated wind) that drive storm surges and the proximity of the two sites. The storm surge levels at each site were then compared which resulted in a mean difference of 1 cm and a standard deviation of 39 cm (Figure 5). A 48 hour moving average of storm surge levels was calculated, which clearly shows that Saint John experiences slightly higher storm surge events (approximately 1 cm on average) than Digby (Figure 5).

This is probably due to the fact that Digby is situated in the Annapolis Basin and is somewhat sheltered. Based on these results, it was deemed reasonable to use the Saint John water level record to estimate water levels and return periods for storm surge events in the Annapolis Basin. The significant wave height is not the same as the wave run-up however.

Figure 5. Comparison of water levels at Saint John and Digby for the period of January to March, 1970. Top panel: the observed and predicted water level and calculated storm surge (m) for Saint John, NB. Middle panel: the observed and predicted water level and calculated storm surge (m) for Digby, NS. Bottom panel: comparison of the storm surges for Saint John (shades of blue) and Digby (shades of red) with a 48 hour mean (heavy lines) to reduce high frequency noise and the difference between them (heavy black line).

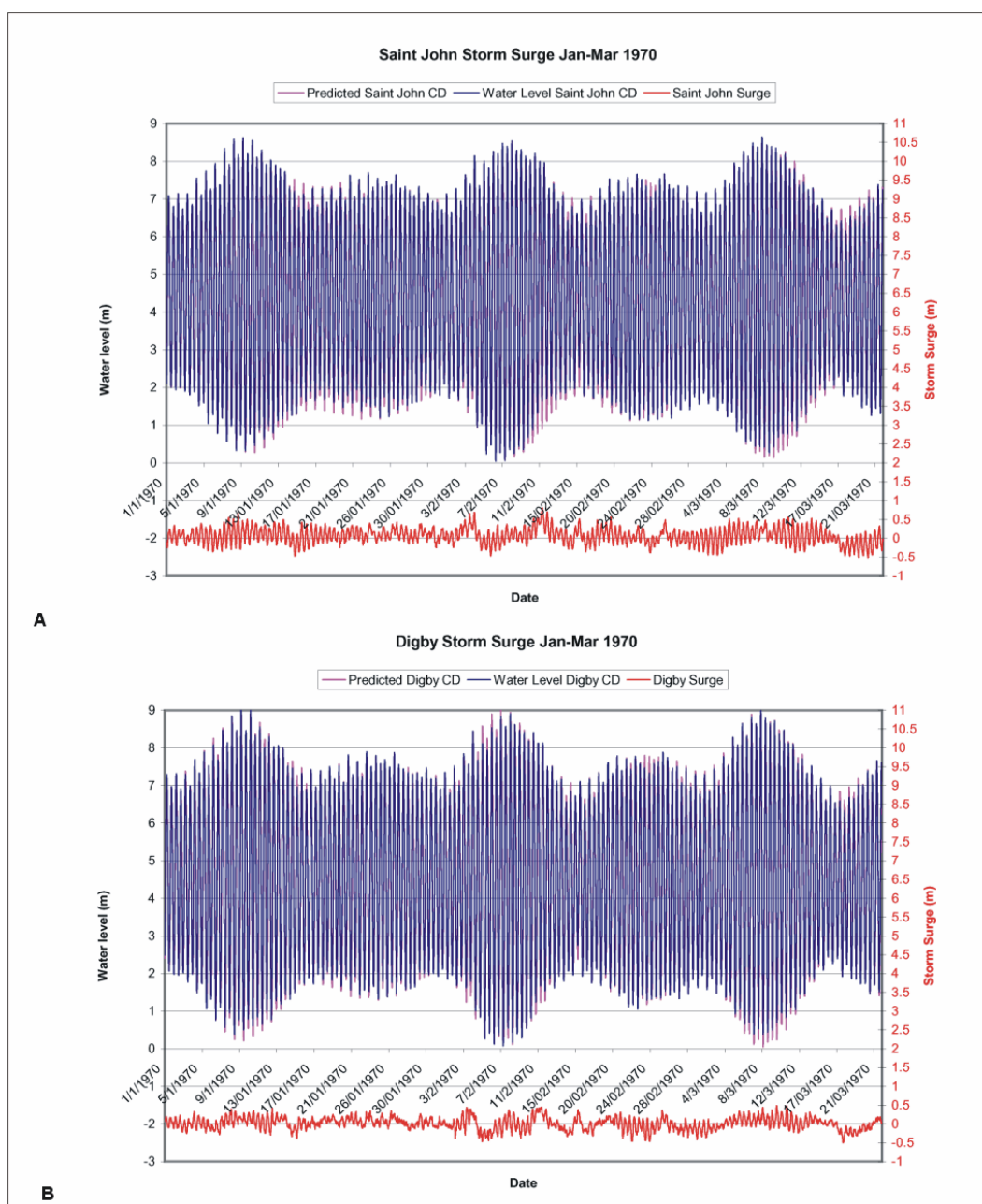
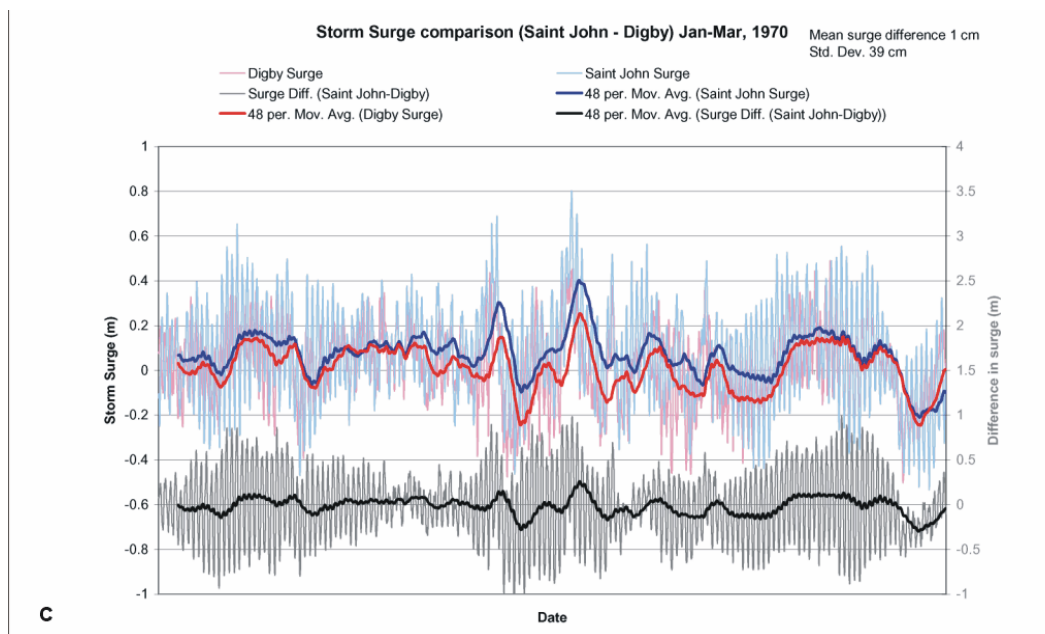


Figure 5. Cont.

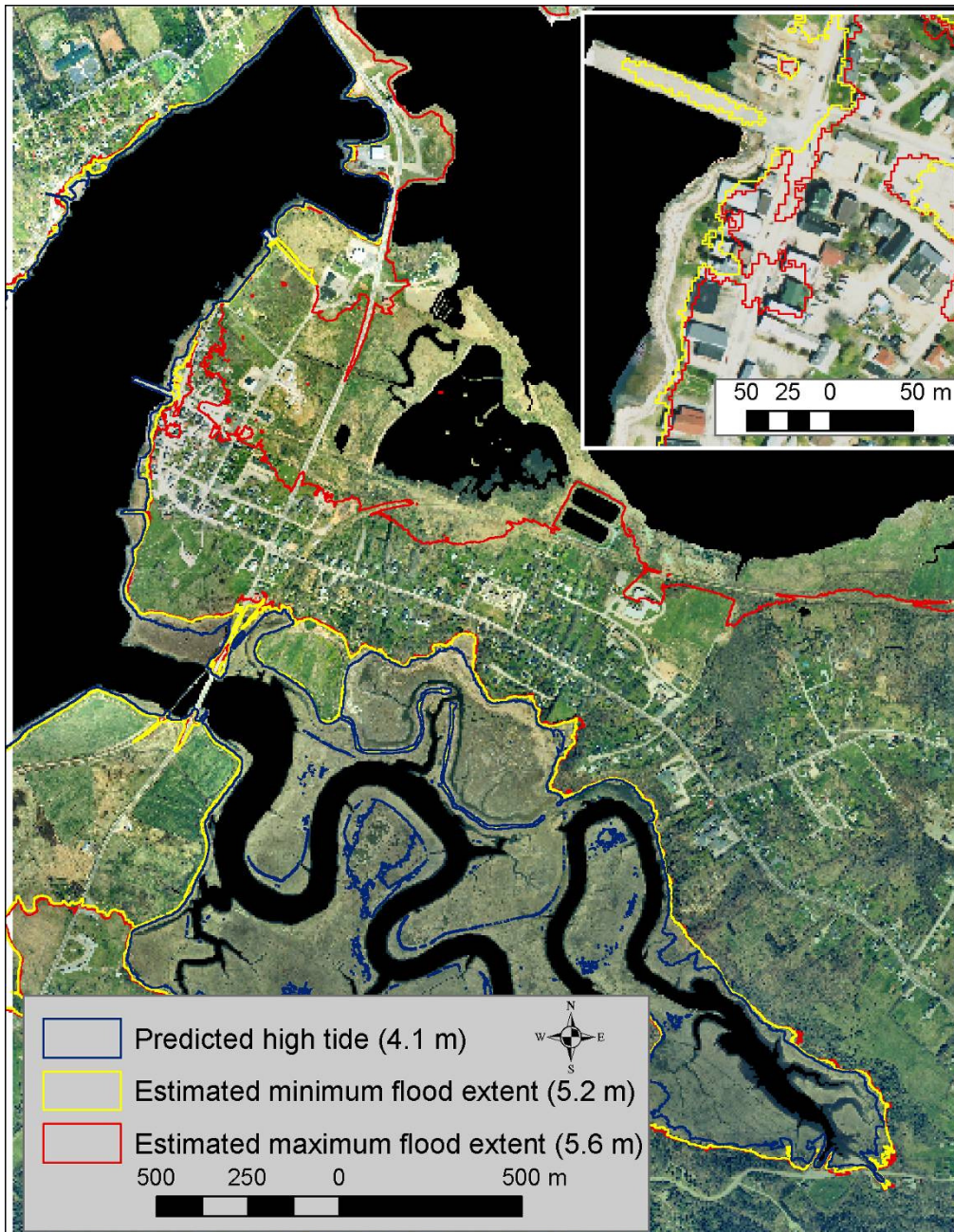


3.4. Flood Inundation Mapping, Sea-Level Rise and Return Periods

It is difficult to validate any flood inundation model, especially when using future predictions. In order to test if the water levels translated from Saint John to the Annapolis Basin were accurate and the DEM was sufficient, the benchmark Groundhog Day storm was used to test the model. The observed water level was subtracted from the predicted tide water level for Saint John, resulting in storm surge of approximately 1.3 m. This value is close to the reported value of 1.5 m by [50] for Saint John. To translate this information from Saint John across the Bay of Fundy to the Annapolis Basin, the value 1.5 m was added to the predicted high tide level for Digby during the Groundhog Day storm in order to determine the total water level. This value was used to estimate storm surge and wave run-up within the Annapolis Basin, considering the Annapolis Basin storm surges are usually less than those experienced in Saint John (Figure 6). The predicted high tide water level of 8.5 m above Chart Datum (CD) or 4.1 m orthometric (using Digby CGVD28-CD offset of 4.39 m) was used for Annapolis Royal with an increased water level of 1.5 m, producing a total water level of 5.6 m. The difference between storm surges in Saint John and the Annapolis Basin indicated a standard deviation of 40 cm, thus a water level of 5.2 m was also generated to give a minimum estimate of the flood extent. The resultant water levels inundated some key areas within the town including lower George Street (inset map Figure 6), and overtopped the government wharf (Figure 6). The upper level of 5.6 m predicts that Highway 1 between the causeway and the town would have been inundated; however the newspaper reports on the extent of the flood did not mention this. The lower water level of 5.2 m partially covers the wharf and approaches the landmarks described in the newspaper reports. These results are consistent with the variance (standard deviation of 0.4 m) in storm surge levels observed between Digby and Saint John. Thus, a water level of between 5.2 and 5.6 m orthometric height appears to accurately represent the range of flood conditions observed in Annapolis Royal during the Groundhog Day storm. A median value of 5.4 m was chosen to predict flooding from a similar storm in 2076

under different sea-level rise conditions.

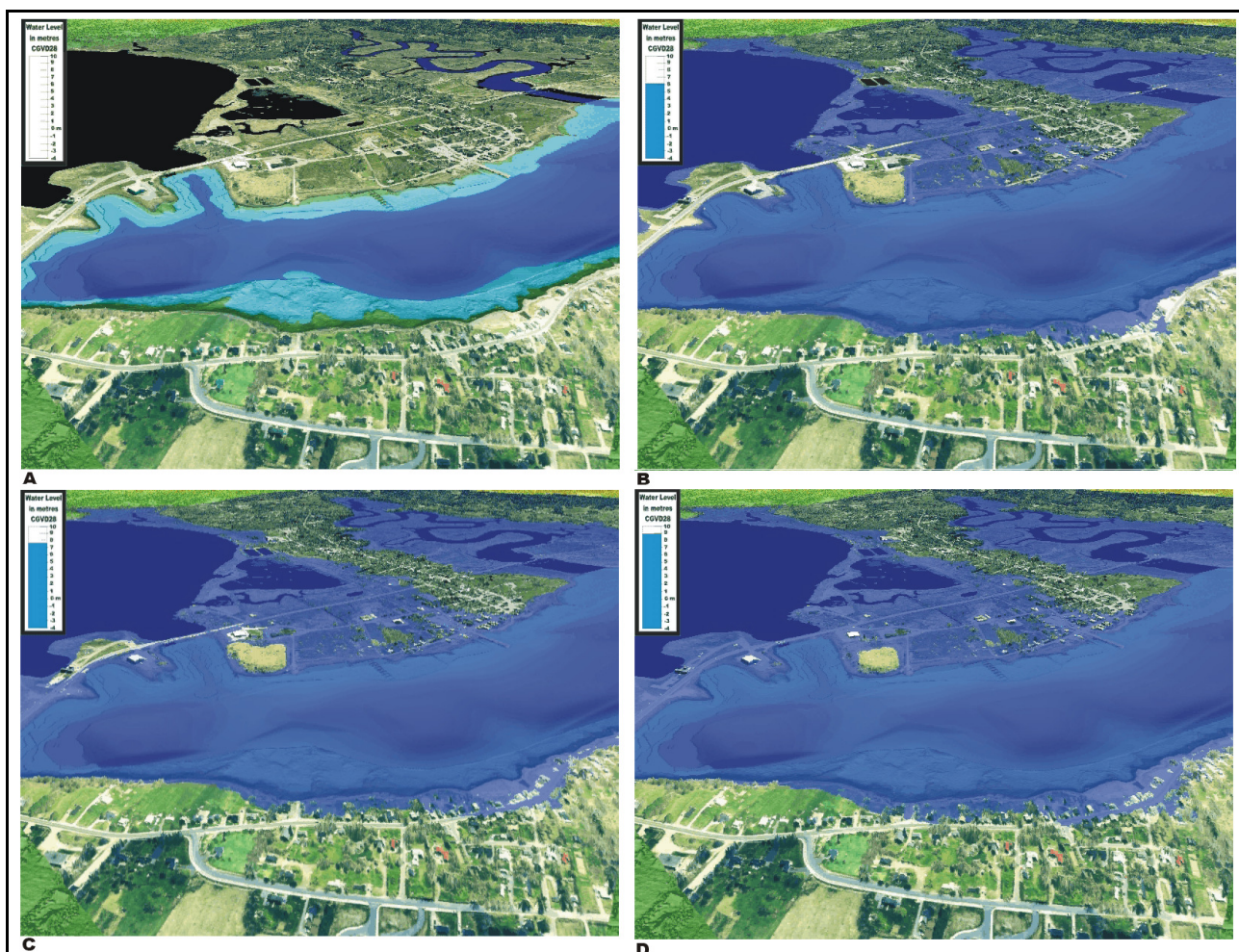
Figure 6. Modeled flood inundation area for a predicted tide (4.1 m) and storm surge; possible water level ranges (5.2–5.6 m) of the Groundhog Day storm, 1976. The background map is a color orthophoto acquired in May 2003.



The results from the Groundhog Day storm model are in sufficient agreement with reported flood extents to confidently predict future flood extents. Water levels were generated in 10 cm increments from -4 m to 9 m orthometric height. A select set of water levels have been used to generate perspective views of the town to demonstrate potential future flooding conditions. These include the current low tide limit during the LiDAR flight (-4 m), the Groundhog Day storm in 100 years at a RSL rate of 80 cm/century (6.2 m), in 100 years at an upper estimate RSL rate of 220 cm/century (7.6 m), and finally the highest astronomical tide plus a 2 m storm surge and the RSL rate of 220 cm/century in

100 years (9.0 m) (Figures 7 and 8). The perspective views were generated by overlaying the May 2003 orthophoto on the LiDAR DSM and superimposing the flood inundation level in blue. The viewing angle for the perspectives is toward the southeast (Figure 7).

Figure 7. Perspective views of Annapolis Royal looking southeast. May 2003 color orthophoto and bathymetric data overlaid on the LiDAR DSM. (A) low tide (−4 m); (B) Groundhog Day storm in 100 years with a conservative RSL of 80 cm, (6.2 m); (C) Groundhog Day storm in 100 years with a potential RSL of 220 cm, (7.6 m); (D) highest predicted tide with a 2 m storm surge in 100 years with a potential RSL of 220 cm, (9.0 m).



The perspective views in Figure 7 are very useful to demonstrate to the public and municipal officials where the water may inundate with the rising sea-level rise in the future. These views have been extracted from a series of frames in which the sea-level was increased in 10 cm increments. The entire set of frames were used to construct animations that are useful for demonstrating the path the water will take as the sea-level rises. In the case of Annapolis Royal, the water moves up a ditch system and around an abandoned protective dyke along the water front. The ditch is located to the right of the isolated land area in the middle of the scene in Figure 7(D). As the sea-level increases, eventually the water inundates the land behind the dyke and crosses the road, separating some key emergency services such as the fire department from the hospital. However, these views are not

suitable for mapping or planning purposes and a series of maps were constructed defining the extent of the flood inundation (Figure 8).

Figure 8. Different possible sea-level rise projections of the Groundhog Day storm in 100 years. Digital orthophoto (May 2003) of Annapolis Royal with a vector outline of flood inundation layers based on the LiDAR DEM.



The risk of these water levels was calculated using the Water Modeler software and the time series of water levels from the Saint John tide gauge record. As a result of the analysis of coincident water level records from Saint John and Digby (Annapolis Basin) (Figure 5), the long time series at Saint John can be used to estimate the water level and return periods in Annapolis Royal. The benchmark storm was used to illustrate the possible effects of climate change and sea-level rise on storm return

periods (Table 1). Municipal planners are often interested in the 50 and 100 year flood level for restrictions on development. Water Modeler was used to assess the water level for the 10 and 100 year return period events based on the Saint John records. However, the water levels calculated for return periods of 50 and 100 years based on the Saint John records should be considered as estimates with a possible uncertainty of ± 39 cm at Annapolis Royal (Table 2).

Table 1. Return periods (years) and probabilities of occurrence of the Groundhog Day storm water level (4.95 m) under current and projected sea-level rise conditions (from [35,41,50]). The return period has been rounded to the nearest year.

Probability	Return period (years) RSL = 0.36 cm/year (current)	Return period (years) RSL = 0.80 cm/year (climate change)	Return period (years) RSL = 2.20 cm/year (climate change)
Average (~65–75 %)	30	23	14
100 %	66	44	22

Table 2. Water levels (m) for return periods of the 50 and 100 year events with different sea-level rise projections (from [35,41,50]). The water level has been rounded to the nearest decimeter.

Return Period (Years)	Water level (m) with RSL = 0.36 cm/year (current)	Water level (m) with RSL = 0.80 cm/year (climate change)	Water level (m) with RSL = 2.20 cm/year (climate change)
50	4.8	4.9	5.6
100	5.1	5.5	6.8

4. Discussion and Conclusions

Annapolis Royal is vulnerable to storm surges and a rising sea-level. Although the Bay of Fundy has some of the largest tides in the world and the probabilities of a significant storm surge occurring on a high tide may be lower than some other regions of the Maritimes, past events such as the Groundhog Day storm of 1976 prove that this region is not immune to such events. This region of Canada experiences storm surges of 1–2 m periodically. Prior to the collection of LiDAR and the construction of high-resolution DEMs with accuracies better than 30 cm, existing digital mapping was not sufficient to accurately map flood risk for most communities, including Annapolis Royal. The LiDAR DEM provides sufficient detail to construct accurate flood inundation maps and when combined with probability statistics from long-term tide-gauge records, flood risk maps were produced. Climate change will impact sea-levels on a global scale and the local crustal conditions in this region will add to the problem as a result of subsidence, thus increasing relative sea-level rise. Currently the lower sections of the town of Annapolis Royal, particularly lower George St. and the government wharf, experience flooding during extreme high tide events in the absence of storms. When storm surges and high winds and waves occur with higher than usual tides, this area of the town is most vulnerable to flooding. The occurrence of these extreme high tides can be predicted based on astronomical

conditions. The most significant high tides occur on Soras cycles, of which the most famous storm to cause coastal flooding in the Bay of Fundy region was the “Saxby Gale” of 1869. The predicted water level at Annapolis Royal during the next Soras cycle will peak at 9.14 m CD (4.75 m orthometric) on May 7, 2012. Other time periods where the predicted water level will be above 9 m CD will occur on April 8–9, May 6–7, June 5, October 16, November 14–16, and December 14–15 of that year. If coastal development is planned to take place in any of the risk areas mapped when simulating the Groundhog Day storm, then significant protective structures such as dykes must be constructed to prevent water from the basin or Annapolis River from flooding these areas.

Acknowledgements

I would like to thank several individuals and groups for their assistance during this project. Angela Templin, research intern who initially worked on the Annapolis Royal flood risk project. Roger Mosher from the Applied Geomatics Research Group, for providing assistance and guidance with the Water Modeler software to compute return period probabilities and the SWAN wave modeling. Natacha Bernier and Keith Thompson, Dalhousie University Oceanography Dept. for providing a copy of Bernier’s PhD thesis. The Odell House for providing historical photos of the town and providing access and copies of the Annapolis County Spectator for the Groundhog Day storm coverage. Charles Hanna for providing information and advice on sea-level rise predictions for the Bay of Fundy. George Parkes for providing information and insights into the Groundhog Day storm and storm surges in the Bay of Fundy. David Mossman for providing reprints on past storm events in the Bay of Fundy. Charles O’Reilly for providing the chart datum—CGVD28 relationships for the different regions in the study. Denise Sullivan, Andy Sharp and Steve Hawbolt from CARP and other residents of Annapolis Royal for providing insights into the flood extent of the Groundhog Day storm. Tam Hill & Jeff Parks for their project management and involving us in the project.

References

1. Flood, M.; Gutelius, B. Commercial implications of topographic terrain mapping using scanning airborne laser radar. *Photogramm. Eng. Remote Sensing* **1997**, *4*, 327-366.
2. Wehr, A.; Lohr, U. Airborne laser scanning—An introduction and overview. *ISPRS J. Photogramm. Remote Sens.* **1999**, *54*, 68-82.
3. Meng, X.; Currit, N.; Zhao, K. Ground filtering algorithms for airborne LiDAR data: A review of critical issues. *Remote Sensing* **2010**, *2*, 833-860.
4. Kraus, K.; Pfeifer, N. A new method for surface reconstruction from laser scanning data. In *International Archives of Photogrammetry, Remote Sensing and Spatial Information Sciences*, ISPRS: Vienna, Austria, 1997; Volume 32, Part 3-2W3, pp. 80-86.
5. Kraus, K.; Pfeifer, N. Determination of terrain models in wooded areas with airborne laser scanner data. *ISPRS J. Photogramm. Remote Sens.* **1998**, *53*, 193-203.
6. Vosselman, G. Slope based filtering of laser altimetry data. In *Proceedings of Technical Commission III*, Amsterdam, The Netherlands, July 2000; In *International Archives of Photogrammetry, Remote Sensing and Spatial Information Sciences*, ISPRS: Vienna, Austria, 2000; Volume 33, Part B4, pp. 958-064.

7. Axelsson, P. DEM generation from laser scanner data using adaptive tin methods. In *Proceedings of Technical Commission III*, Amsterdam, The Netherlands, July 2000; In *International Archives of Photogrammetry, Remote Sensing and Spatial Information Sciences*, ISPRS: Vienna, Austria, 2000; Volume 33, Part B3, pp. 85-92.
8. Zhang, K.; Chen, S.; Whitman, D.; Shyu, M.; Yan, J.; Zhang, C. A progressive morphological filter for removing nonground measurements from airborne LIDAR data. *IEEE Trans. GeoSci. Remote Sens.* **2003**, *4*, 872-882.
9. Raber, G.; Jensen, J.R.; Schill, S.R.; Schuckman, K. Creation of digital terrain models using an adaptive LiDAR vegetation point removal process. *Photogramm. Eng. Remote Sensing* **2002**, *68*, 1307-1315.
10. Hodgson, M.E.; Bresnahan, P. Accuracy of airborne LiDAR-derived elevation: Empirical assessment and error budget. *Photogramm. Eng. Remote Sensing* **2004**, *3*, 331-339.
11. Lane, S.; James, T.D.; Pritchard, H. Photogrammetric and laser altimetric reconstruction of water levels for extreme flood event analysis. *Photogramm. Record* **2003**, *18*, 293-307.
12. Bates, P.D.; Marks, K.J.; Horritt, M.S. Optimal use of high-resolution topographic data in flood inundation models. *Hydrol. Process.* **2003**, *17*, 537-557.
13. Cobby, D.M.; Mason, D.C.; Horritt, M.S.; Bates, P.D. Two-dimensional hydraulic flood modeling using a finite-element mesh decomposed according to vegetation and topographic features derived from airborne scanning laser altimetry. *Hydrol. Process.* **2003**, *17*, 1979-2000.
14. Haile, A.T.; Rientjes, T.H.M. Effect of LiDAR DEM resolution in flood modeling: A model sensitivity study for the city of Tegucigalpa, Honduras. In *Proceedings of ISPRS WG III/3, III/4, V/3 Workshop "Laser scanning 2005"*, Enschede, The Netherlands, September 12–14, 2005; pp. 168-173.
15. Mason, D.C.; Horritt M.S.; Hunter, N.M.; Bates, P.D. Use of fused airborne scanning laser altimetry and digital map data for urban flood modeling. *Hydrol. Process.* **2007**, *21*, 1436-1447.
16. Raber, G.; Jensen, J.R.; Hodgson, M.E.; Tullis, J.A.; Davis, B.A.; Berglund, J. Impact of LiDAR nominal post-spacing on DEM accuracy and flood zone delineation. *Photogramm. Eng. Remote Sensing* **2007**, *73*, 793-804.
17. Gutierrez, R.; Gibeaut, J.C.; Smyth, R.C.; Hepner, T.L.; Andrews, J.R. Precise airborne LiDAR surveying for coastal research and geohazards applications. In *Proceedings of the ISPRS Workshop "Land Surface Mapping and Characterization Using Laser Altimetry"*, Annapolis, MD, USA, October 22–24, 2001; In *International Archives of Photogrammetry, Remote Sensing and Spatial Information Sciences*, ISPRS: Vienna, Austria, 2001; Volume 34-3/W4, pp. 22-24.
18. Webster, T.L.; Forbes, D.L.; Dickie, S.; Shreenan, R. Using topographic LiDAR to map flood risk from storm surge events for Charlottetown, Prince Edward Island, Canada. *Canad. J. Remote Sens.* **2004**, *30*, 54-76.
19. Webster, T.L.; Christian, M.; Sangster, C.; Kingston, D. High-resolution elevation and image data within the Bay of Fundy Coastal Zone, Nova Scotia, Canada. In *GIS for Coastal Zone Management*; Bartlett, D., Smith, J., Eds.; CRC Press: Boca Raton, FL, USA, 2005; pp. 195-218.
20. Webster, T.L.; Forbes, D.L.; MacKinnon, E.; Roberts, D. Floodrisk mapping for storm surge events and sea-level rise in Southeast New Brunswick. *Canad. J. Remote Sens.* **2006**, *32*, 194-211.

21. Webster, T.L.; Forbes, D.L. Airborne laser altimetry for predictive modelling of coastal storm surge flooding. In *Remote Sensing of Aquatic Ecosystem Processes, Science and Management Applications*; LeDrew, E., Richardson, L., Eds.; Springer: Dordrecht, The Netherlands, 2006; pp. 157-180.
22. Webster, T.; Stiff, D. The prediction and mapping of coastal flood risk associated with storm surge events and long-term sea level changes. In *Risk Analysis VI Simulations and Hazard Mitigation*; Brebbia, C.A., Beriatos, E., Eds.; WIT Press: Wessex, UK, 2008; pp. 129-139.
23. Webster, T.L.; Mosher, R.; Pearson, M. A coastal zone decision support system to generate flood risk maps from storm surge events and sea level rise. *Geomatica* **2008**, *62*, 393-406.
24. Poulter, B.; Halpin, P.N. Raster modeling of coastal flooding from sea-level rise. *Int. J. Geogr. Inf. Sci.* **2008**, *22*, 167-182.
25. Klemas, V. The role of remote sensing in predicting and determining coastal storm impacts. *J. Coast. Res.* **2009**, *6*, 1264-1275.
26. Krabill, W.B.; Wright, C.; Swift, R.; Frederick, E.; Manizade, S.; Yungel, J.; Martin, C.; Sonntag, J.; Duffy, M.; Brock, J. Airborne laser mapping of assateague national seashore beach. *Photogramm. Eng. Remote Sensing* **1999**, *66*, 65-71.
27. Brock, J.C.; Wright, C.W.; Sallenger, A.H.; Krabill, W.B.; Swift, R.N. Basis and methods of NASA airborne topographic mapper LIDAR surveys for coastal studies. *J. Coast. Res.* **2002**, *18*, 1-13.
28. Stockdon, H.F.; Sallenger, A.H.; List, J.H.; Holman, R.A. Estimation of shoreline position and change using airborne topographic LIDAR data. *J. Coast. Res.* **2002**, *18*, 502-513.
29. Sallenger, A.H., Jr; Krabill, W.B.; Swift, R.N.; Brock, J. Evaluation of airborne topographic LiDAR for quantifying beach changes. *J. Coast. Res.* **2003**, *19*, 125-133.
30. Robertson, W.V.; Whitman, D.; Zhang, K.; Leatherman, S.P. Mapping shoreline position using airborne laser altimetry. *J. Coast. Res.* **2004**, *20*, 884-892.
31. Morton, R.A.; Miller, T.L.; Moore, L.J. Historical shoreline changes along the US Gulf of Mexico: A summary of recent shoreline comparisons and analysis. *J. Coast. Res.* **2004**, *4*, 704-709.
32. Zhou, G.; Xie, M. Coastal 3-D morphological change analysis using LiDAR series data: A case study of Assateague Island National Seashore. *J. Coast. Res.* **2009**, *2*, 435-447.
33. Shaw, J.; Taylor, R.B.; Forbes, D.L.; Ruz, M-H.; Solomon, S. *Sensitivity of the Canadian Coast to Sea-Level Rise*; Geological Survey of Canada, Bulletin 505; Natural Resources Canada: Ottawa, ON, Canada, 1994; p. 114.
34. McCulloch, M.M.; Forbes, D.L.; Shaw, R.W.; and the CCAF A041 Scientific Team. *Coastal Impacts of Climate Change and Sea-Level Rise on Prince Edward Island*; Open File 4261; Geological Survey of Canada, Natural Resources Canada: Ottawa, ON, Canada, 2002.
35. Church, J.A.; Gregory, J.M.; Huybrechts, P.; Kuhn, M.; Lambeck, K.; Nhuan, M.T.; Qin, D.; Woodworth, P.L. Changes in sea level. In *Climate Change 2001: The Scientific Basis. Contribution of Working Group I to the Third Assessment Report of the Intergovernmental Panel on Climate Change*; Cambridge University Press: Cambridge, UK, 2001; pp. 639-693.

36. Meehl, G.A.; Stocker, T.F.; Collins, W.D.; Friedlingstein, P.; Gaye, A.T.; Gregory, J.M.; Kitoh, A.; Knutti, R.; Murphy, J.M.; Noda, A.; Raper, S.C.B.; Watterson, I.G.; Weaver, A.J.; Zhao, Z.-C. Global climate projections. In *Climate Change 2007: The Physical Science Basis. Contribution of Working Group I to the Fourth Assessment Report of the Intergovernmental Panel on Climate Change*; Solomon, S., Qin, D., Manning, M., Chen, Z., Marquis, M., Averyt, K.B., Tignor, M., Miller, H.L., Eds.; Cambridge University Press: Cambridge, UK and New York, NY, USA, 2007; pp. 1-844.
37. Bindoff, N.L.; Willebrand, J.; Artale, V.; Cazenave, A.; Gregory, J.; Gulev, S.; Hanawa, K.; Le Quéré, C.; Levitus, S.; Nojiri, Y.; Shum, C.K.; Talley, L.D.; Unnikrishnan, A. Observations: Oceanic climate change and sea level. In *Climate Change 2007: The Physical Science Basis. Contribution of Working Group I to the Fourth Assessment Report of the Intergovernmental Panel on Climate Change*; Solomon, S., Qin, D., Manning, M., Chen, Z., Marquis, M., Averyt, K.B., Tignor, M., Miller, H.L., Eds.; Cambridge University Press: Cambridge, UK and New York, NY, USA, 2007; pp. 1-429.
38. Forbes, D.L.; Manson, G.K.; Charles, J.; Thompson, K.R.; Taylor, R.B. *Halifax Harbour Extreme Water levels in the Context of Climate Change: Scenarios for a 100-Year Planning Horizon*; Open File 6346; Geological Survey of Canada, Natural Resources Canada: Ottawa, ON, Canada, 2009; pp. 1-21.
39. Rhamstorf, S.; Cazenave, A.; Church, J.A.; Hansen, J.E.; Keeling, R.F.; Parker, D.E.; Somerville, R.C.J. Recent climate observations compared to projections. *Science* **2007**, *316*, 709.
40. Levermann, A.; Griesel, A.; Hofmann, M.; Montoya, M.; Rahmstorf, S. Dynamic sea level changes following changes in the thermohaline circulation. *Clim. Dynam.* **2005**, *24*, 347-354.
41. Vermeer, M.; Rahmstorf, S. Global sea level linked to global temperature. *Proc. Nat. Acad. Sci. USA* **2009**, doi: 10.1073/pnas.0907765106.
42. Rahmstorf, S. A semiempirical approach to projecting future sea-level rise. *Science* **2007**, *315*, 368-370.
43. Bernier, N.B.; Thompson, K.R. Predicting the frequency of storm surges and extreme sea levels in the Northwest Atlantic. *J. Geophys. Res.* **2006**, doi:10.1029/2005JC003168.
44. Belbin, J.; Clyburn, D. *Tidal Surge Project: The Coastal Flooding Component of the Annapolis Climate Change Outreach Project*; Unpublished Report for the Clean Annapolis River Project, 1998; Available online: <http://c-ciarn.dal.ca/workshops/3/presentations/Belbin.pdf> (accessed on 20 August 2010).
45. Booij, N.; Ris, R.C.; Holthuijsen, L.H. A third-generation wave model for coastal regions 1. Model description and validation. *J. Geophys. Res.* **1999**, *104*, 7649-7666.
46. Abraham, J.; Parkes, G.; Bowyer, P. The transition of the “Saxby Gale” into an extratropical storm. In *Proceedings of the 23rd Conference on Hurricanes and Tropical Meteorology*, American Meteorological Society, Dallas, TX, USA, 1999; pp. 795-798.
47. Desplanque, C.; Mossman, D. Tides and their seminal impact on the geology, geography, history, and socio-economics of the Bay of Fundy, eastern Canada. *Atlantic Geol.* **2004**, *40*, 1-130.
48. MacDonald, A. Winds of Change Severe Weather in The Annapolis Valley. Unpublished Thesis, Bachelor of Arts with Honours in History, Acadia University, Wolfville, NS, Canada, 2006.

49. Parkes, G.; Ketch, L.; O'Reilly, C. Storm surge events in the Maritimes. In *Procedures of the Canadian Coastal Conference*, Guelph, ON, Canada, 1997; pp. 115-129.
50. Desplanque, C.; Mossman, D. Storm tides of the fundy. *The Geogr. Rev.* **1999**, *89*, 23-33.
51. Brennen, R.; Webster, T.L. Object oriented land cover classification of LiDAR derived surfaces. *Canad. J. Remote Sens.* **2006**, *32*, 167-172.
52. Webster, T.L.; Dias, G. An automated GIS produce for comparing GPS and proximal LIDAR elevations. *Comput.Geosci.* **2006**, *32*, 713-726.
53. Webster, T.L. LIDAR validation using GIS: A case study comparison between two LIDAR collection methods. *GeoCarto Int.* **2005**, *20*, 11-19.
54. Peltier, W.R. Global glacial isostasy and the surface of the ice-age earth: The ice-5G (VM2) model and Grace. *Ann. Rev. Earth Planetary Sci.* **2004**, *32*, 111-149.
55. Godin G. Possibility of rapid changes in the tide of the Bay of Fundy, based on a scrutiny of the records from Saint John. *Continental Shelf Res.* **1992**, *12*, 327-338.

© 2010 by the authors; licensee MDPI, Basel, Switzerland. This article is an open access article distributed under the terms and conditions of the Creative Commons Attribution license (<http://creativecommons.org/licenses/by/3.0/>).